



Low driving voltage band-filling-based III-V-on-silicon electroabsorption modulator

Qiangsheng Huang, Yingchen Wu, Keqi Ma, Jianhao Zhang, Weiqiang Xie, Xin Fu, Yaocheng Shi, Kaixuan Chen, Jian-Jun He, Dries Van Thourhout, Gunther Roelkens, Liu Liu, and Sailing He

Citation: [Applied Physics Letters](#) **108**, 141104 (2016); doi: 10.1063/1.4945666

View online: <http://dx.doi.org/10.1063/1.4945666>

View Table of Contents: <http://scitation.aip.org/content/aip/journal/apl/108/14?ver=pdfcov>

Published by the [AIP Publishing](#)

Articles you may be interested in

[Low-voltage electro-absorption optical modulator based on slow-light Bragg reflector waveguide](#)

Appl. Phys. Lett. **102**, 031118 (2013); 10.1063/1.4789533

[Efficient infrared electroabsorption with 1 V applied voltage swing using intersubband transitions](#)

Appl. Phys. Lett. **93**, 191101 (2008); 10.1063/1.3013360

[Blue quantum electroabsorption modulators based on reversed quantum confined Stark effect with blueshift](#)

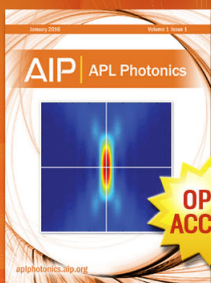
Appl. Phys. Lett. **90**, 011101 (2007); 10.1063/1.2424642

[Ultraviolet electroabsorption modulator based on Al Ga N/Ga N multiple quantum wells](#)

J. Appl. Phys. **97**, 123515 (2005); 10.1063/1.1937471

[Monolithic intracavity laser-modulator device fabrication using postgrowth processing of 1.55 \$\mu\text{m}\$ heterostructures](#)

Appl. Phys. Lett. **79**, 3582 (2001); 10.1063/1.1421234



Launching in 2016!
The future of applied photonics research is here

AIP | APL
Photonics

Low driving voltage band-filling-based III-V-on-silicon electroabsorption modulator

Qiangsheng Huang,^{1,2} Yingchen Wu,^{2,3} Keqi Ma,¹ Jianhao Zhang,¹ Weiqiang Xie,² Xin Fu,^{1,2} Yaocheng Shi,¹ Kaixuan Chen,⁴ Jian-Jun He,³ Dries Van Thourhout,² Gunther Roelkens,² Liu Liu,^{4,a)} and Sailing He^{1,4,a)}

¹Centre for Optical and Electromagnetic Research, State Key Laboratory for Modern Optical Instrumentation, Zhejiang University, Hangzhou 310058, China

²Photonics Research Group, Department of Information Technology, Ghent University-IMEC, Ghent B-9000, Belgium

³State Key Laboratory of Modern Optical Instrumentation, Centre for Integrated Optoelectronics, Department of Optical Engineering, Zhejiang University, Hangzhou 310027, China

⁴ZJU-SCNU Joint Research Center of Photonics, Centre for Optical and Electromagnetic Research, South China Academy of Advanced Optoelectronics, Science Building No. 5, South China Normal University, Higher-Education Mega-Center, Guangzhou 510006, China

(Received 28 January 2016; accepted 25 March 2016; published online 5 April 2016)

In this paper, a method for realizing a low driving voltage electroabsorption modulator based on the band-filling effect is demonstrated. The InP-based electroabsorption modulator is integrated using divinylsiloxane-bis-benzocyclobutene adhesive bonding on a silicon-on-insulator waveguide platform. When the electroabsorption modulator is forward biased, the band-filling effect occurs, which leads to a blue shift of the exciton absorption spectrum, while the absorption strength stays almost constant. In static operation, an extinction ratio of more than 20 dB with 100 mV bias variation is obtained in an 80 μm long device. In dynamic operation, 1.25 Gbps modulation with a 6.3 dB extinction ratio is obtained using only a 50 mV peak-to-peak driving voltage. The band-filling effect provides a method for realizing ultra-low-driving-voltage electroabsorption modulators. © 2016 AIP Publishing LLC. [<http://dx.doi.org/10.1063/1.4945666>]

Quantum-confined Stark effect (QCSE) based electroabsorption modulators (EAM) exhibit high speed, low energy consumption, relatively high extinction ratio, and small footprint.^{1,2} These features make EAMs widely used in optical communications. In addition, the electroabsorption effect can also be used to build a high speed photodetector, which possesses a similar structure as that of an EAM.³ This dual function property enables, e.g., on-chip optical transceivers⁴ and compact optoelectronic oscillators (OEO).⁵ Recently, silicon photonics integrated with electronic devices fabricated in complementary metal-oxide semiconductor (CMOS) production lines has become an enabling technology for the realization of integrated optical systems.^{6,7} High speed InP-based EAMs have also been successfully implemented in silicon photonic circuits through hybrid integration technology.^{1,4,8,9} However, for silicon photonics, it is important to reduce the power consumption. Because the transition energy consumed by an EAM is proportional to the driving voltage squared,¹ a low driving voltage EAM is required in silicon photonics. On the other hand, an EAM directly driven by the low voltage swing signal from an advanced digital logical CMOS driver can also save the energy consumption from the electrical signal amplifier. Recently, sub-100 mV driving voltage silicon modulators based on a high Q microring resonator or a photonic crystal cavity have been demonstrated.^{10,11} However, those devices

are very sensitive to fabrication imperfections and cannot be used as photodetectors. For QCSE based EAMs, it is challenging to reduce the driving voltage without an increase in the modulator size and insertion loss. Even when using a complex slow-light Bragg waveguide to enhance light-matter interaction,¹² it is still hard to integrate with silicon photonics and reduce the driving voltage to the level of silicon modulators. Therefore, it is desirable to find a simple way to reduce the driving voltage without requiring complex fabrication procedures.

The band-filling effect in modulation-doped multiple quantum-wells (MQWs) has been studied since the 1980s.¹³ The band-filling effect, whereby the conduction subbands are filled with a two-dimensional (2D) electron gas, results in a blue shift of the absorption edge. By controlling the bias voltage, the electron concentrations in the MQWs region can be adjusted. In this way, both refractive index and absorption edge in the MQW can be controlled by the bias voltage through the band-filling effect. This effect has not only been used in Mach-Zehnder interferometer based modulator^{14,15} but also exploited in 100 mV driven active Q-switching lasers with modulation-doped quantum wells.¹⁶

In this paper, we demonstrate an EAM based on the band-filling effect, operation at 1.55 μm . Although the speed of the presented modulator is not fast (limited by carrier lifetime) compared to the QCSE based EAMs, the drive voltage is reduced below 100 mV, which makes it very promising for low power consumption. The EAM is bonded on and coupled to a silicon-on-insulator (SOI) waveguide circuit,

^{a)}Authors to whom correspondence should be addressed. Electronic addresses: sailing@jorcep.org and liu.liu@coer-scnu.org

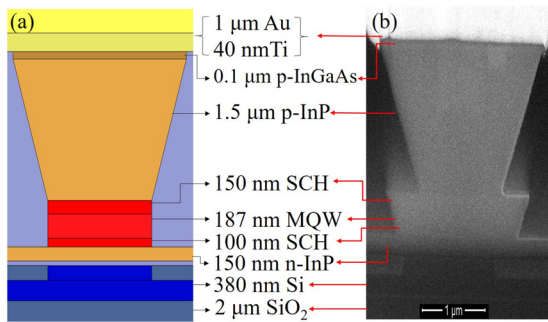


FIG. 1. (a) Cross-sectional view of the EAM bonded on SOI. (b) SEM image of the cross-section of the fabricated III-V/Si hybrid waveguide.

which makes it possible to be directly combined with complex passive silicon photonic circuits and digital CMOS drives.

Fig. 1 shows the cross-sectional view of the EAM integrated on SOI using divinylsiloxane-bis-benzocyclobutene (DVS-BCB) adhesive bonding technology.⁸ It consists of a silicon ridge waveguide, a thin bonding layer, and a III-V p-i-n diode. The 380 nm thick silicon ridge waveguide is etched 160 nm deep and planarized using SiO₂. The thin bonding layer includes a 30 nm thick DVS-BCB layer and 15 nm SiO₂. At the top of the III-V p-i-n structure, there is a 100 nm pInGaAs ($1.5 \times 10^{19} \text{ cm}^{-3}$) layer allowing a low resistance metal contact. Below it, there is a 1.5 μm gradually doped (2×10^{18} to $1 \times 10^{18} \text{ cm}^{-3}$) p-InP. In the intrinsic region, an MQW stack is sandwiched between two separate confinement heterostructure layers (SCH) of In_{0.52}Al_{0.16}Ga_{0.32}As. The MQW stack (nominal photoabsorption edge at 1560 nm) consists of 10 compressively strained In_{0.65}Al_{0.09}Ga_{0.26}As quantum wells and 11 tensile strained In_{0.42}Al_{0.17}Ga_{0.39}As barriers. At the bottom of the III-V structure, a 150 nm thin n-InP ($3 \times 10^{18} \text{ cm}^{-3}$) layer is present and is also used as the lateral contact to the ground metal. The detailed epitaxial layer structure is shown in Figs. 1(a) and 1(b).

The fabrication process of this EAM is simpler than that of our previous laser/modulator.^{4,8,9} Thanks to the highly selective wet etching process used, a photoresist mask instead of a SiN hard mask can be used to define the III-V waveguide. In this way, the deposition and etching of SiN hardmask layers by PECVD and Inductively Coupled Plasma Reactive-ion Etching (ICP-RIE), respectively, are avoided. The SOI waveguide circuit is fabricated through an ePIXfab Multi Project Wafer run.¹⁷ The silicon ridge waveguide is 1.5 μm wide. After bonding and removing the InP substrate and sacrificial layer, a photoresist pattern is defined and transferred into the InGaAs layer by wet-etched by

H₃PO₄:H₂O₂:H₂O = 1:1:20 (Fig. 2(a)). Then using the InGaAs pattern as mask, the p-InP waveguide is wet-etched with HCl:H₂O = 1:1, forming an inverted trapezoid with a top width of 2.5 μm and a bottom width of 1.5 μm (Fig. 2(b)). Once again, a photoresist mask pattern is defined and transferred into MQW+SCH layer by wet-etched with Citric:H₂O₂ = 20:1. By controlling the under-etching time, the width of the MQW+SCH region is nominally reduced to 1.5 μm (Fig. 2(c)). The following fabrication process is the same as our previous work in Ref. 8. Figs. 3(a) and 3(b), respectively, show the three-dimensional sketch of the designed lumped electrode EAM and a top-down photograph of a fabricated device. Fig. 1(b) shows the cross section of the fabricated III-V/Si hybrid waveguide structure.

The mode conversion from the silicon ridge waveguide to the hybrid waveguide is achieved by a 45 μm long bi-level taper in III-V material.^{9,18} The silicon ridge waveguide remains 1.5 μm wide under the bi-level taper. In the first part of the taper, the mode is converted from the silicon ridge waveguide mode to that of the hybrid structure without the thick p-InP layer, where the MQW+SCH layers' width laterally is tapered from 0.2 μm to 1.5 μm. The second part of the taper transforms the optical mode into that of the full III-V waveguide, where the p-InP layer is laterally tapered from 0.2 μm to 2.5 μm and the MQW+SCH layers are kept 1.5 μm wide. The simulated coupling efficiency between the silicon ridge waveguide and the hybrid waveguide is around 98%. The optical confinement factor in the ten quantum wells of the hybrid waveguide is around 24%.

The present EAM with InAlGaAs MQWs exhibits a strong and sharp exciton absorption peak at the absorption edge due to its large conduction band offset.² Since the band-to-band continuum transition energy (which is above the exciton transition energy) has a small influence on the absorption edge, we adopt a theoretical model only containing the exciton transition, in order to simplify the calculation of the absorption spectra and the shift of the absorption edge for the EAM.¹⁹ The material parameters of the MQW structure, such as the effective electron/hole mass, Luttinger parameters, and band energy levels, are taken from Ref. 20, taking into account the nominal composition of each layer. The half-linewidth for the absorption peak varies from 1 meV at zero electric field to 1.4 meV at 42 kV/cm, which is taken from the measuring results. The effective mass m^* of the average matrix element is 0.0064 m_0 ,¹⁹ where m_0 is the electron mass.

The simulated exciton absorption spectra for an 80 μm long EAM are shown in Fig. 4. Due to the p-i-n structure used, there is a built-in electric field at 0 V bias. Zero electric field in the intrinsic layer is achieved at a forward bias of

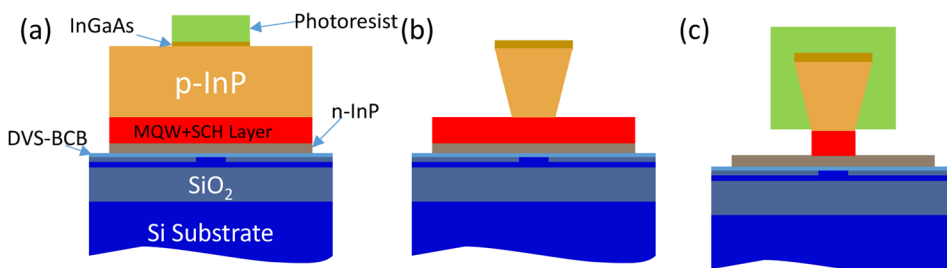


FIG. 2. The fabrication process of the III-V waveguide.

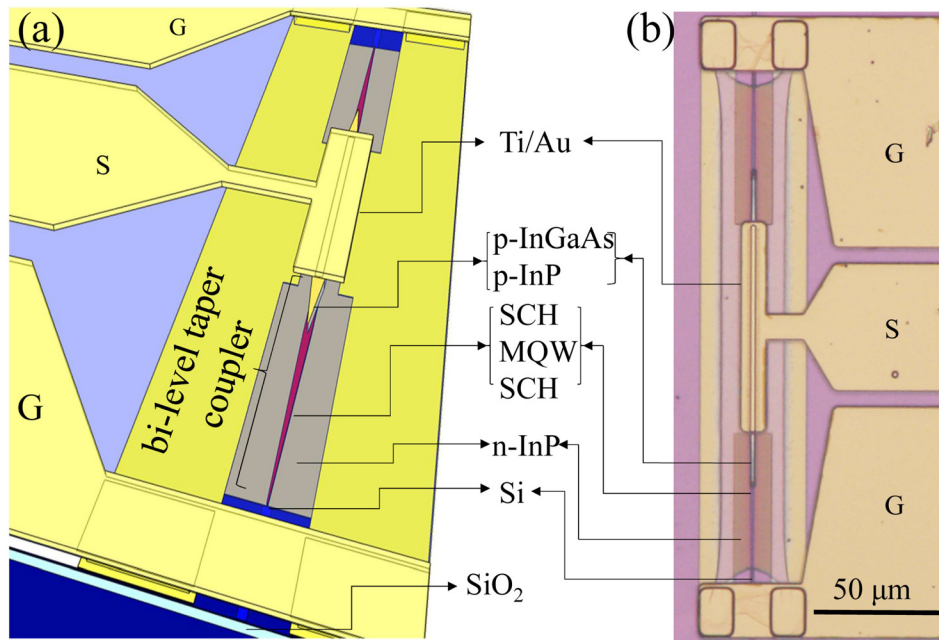


FIG. 3. (a) Three-dimensional sketch of the EAM bonded on SOI. (b) Top microscope image of the III-V/Si hybrid integrated EAM.

0.6 V. Below 0.6 V, the absorption spectra for the EAM are calculated using a QCSE model. The exciton absorption peak red shifts with increasing applied electric field. Due to the decreasing electron-hole overlap integral with increasing electric field, the absorption magnitude decreases. Above 0.6 V, the absorption spectra for the EAM are calculated using a band-filling effect model. The exciton absorption peak blue shifts when more current is injected into the conduction band. Since the electron-hole overlap integral remains almost constant with increasing current density, the absorption does not decrease in magnitude. The exciton transition energy shift ΔE is given by: $\Delta E = (1 + m_e/m_h)E_F$, where E_F is the Fermi energy level for the electrons, and m_e and m_h are the effective electron and hole mass, respectively.¹³ When E_F is substantially higher than the lowest conduction subbands E_1 , E_F increases linearly as the carrier density increases in the quantum well.²¹ Since the carrier density is proportional to the injected current, and the injected current is directly related to the applied voltage, the absorption peak shift is directly proportional to the applied

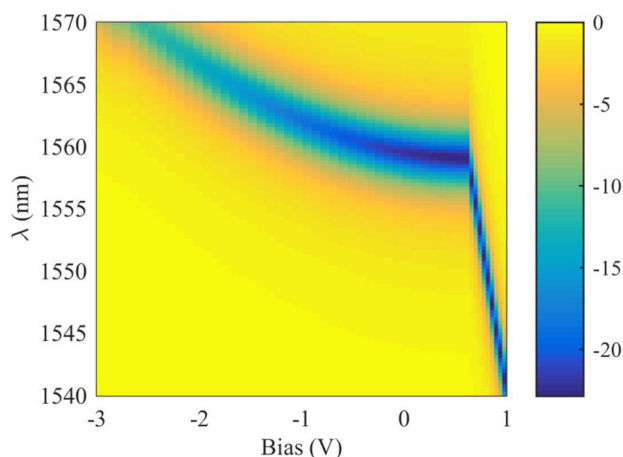


FIG. 4. The simulated exciton absorption spectra (dB) for the 80 μm long EAM with different bias voltages. The strongest absorption is more than 20 dB.

voltage. In this way, by modulating the applied voltage, we can build an efficient modulator.

We first measure the EAMs static performance as a function of bias at 1.55 μm, as shown in Fig. 5(a). The measurement results are normalized to the transmission through a straight waveguide using the same fiber-chip interface. The insertion loss of the EAM is around 5 dB at zero bias, larger than the simulation results. This is attributed to the fact that the width of the MQW+SCH region in the fabricated device is larger than the designed value of 1.5 μm, shown in Fig. 1(b). In this case, the bi-level taper coupler will excite higher order modes and cause unwanted reflection during mode transformation, especially in the first level taper.¹⁸ Fig. 5(a) shows that there are two regimes of absorption variation versus bias voltage. In the reverse bias, the absorption variation is caused by continuum transition absorption (the classic electroabsorption effect). Due to the short device length, the extinction ratio is only around 4 dB with the voltage changing from -1 V to -2 V. In the forward bias, the absorption variation is caused by the exciton transition absorption. The change in absorption is more than 20 dB with only 100 mV bias variation. The measured absorption spectra with bias variation are shown in Fig. 5(b). The exciton peak absorption and shifts are in good agreement with the simulation results shown in Fig. 4. In the forward bias, the blue shift rate of the exciton absorption peak is around 50 nm/V, without a reduction in absorption strength. Therefore, a low driving voltage EAM can be realized in the forward bias.

Next, we measure dynamic performance of the EAM at 1.55 μm. A non-return-to-zero (NRZ) $2^{31}-1$ pseudorandom bit sequence (PRBS) pattern is generated and attenuated to a level of 50 mV swing and then applied to the III-V-on-silicon EAM via a bias-T providing a forward bias of 0.6 V. The modulated light is coupled out to a fiber through a fiber-to-chip grating coupler and amplified by an erbium-doped fiber amplifier (EDFA). The amplified spontaneous emission generated by the EDFA is subsequently filtered out by a narrow optical filter. Eye diagrams are measured using a Tektronix

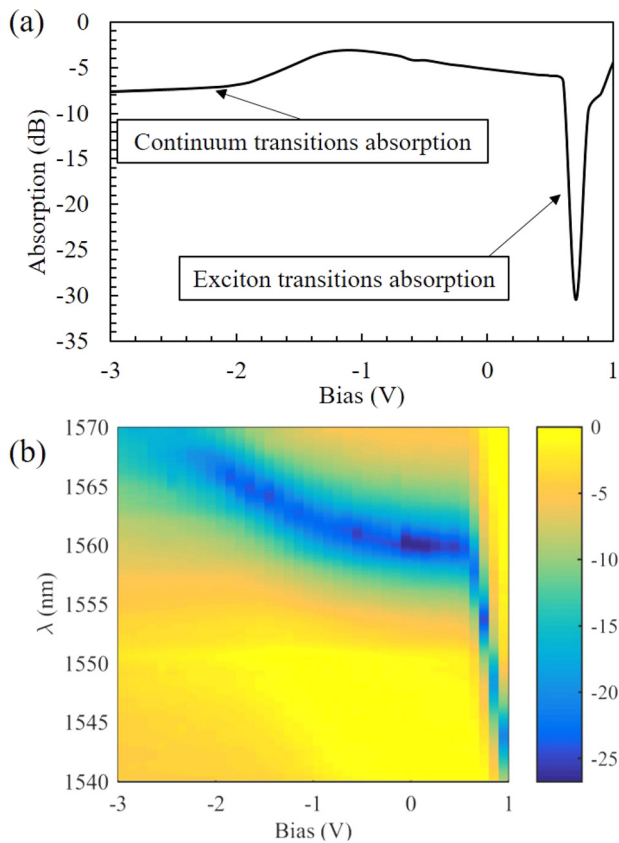
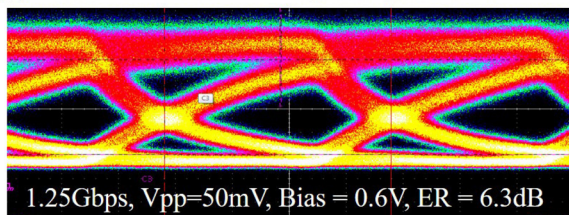


FIG. 5. (a) The bias dependent absorption for the 80 μm long EAM at 1.55 μm . (b) The exciton absorption spectra (dB) for different bias voltages. The strongest absorption is more than 20 dB.

8300A digital series analyzer. The 1.25 Gbps eye diagram of the EAM is shown in Fig. 6(a). The dynamic extinction ratio is 6.3 dB, which is twice as large as the low voltage drive silicon modulators based on tuning the resonant wavelength with the same peak-to-peak voltage.¹¹ The method to calculate the energy consumption of the EAM is presented in Ref. 1. Because the cross-section of our 80 μm long EAM is the same as our previous 100 μm long modulator,⁹ the junction capacitance is estimated to be around 116 fF. The

(a) Exciton transitions absorption, @1550nm



(b) Continuum transitions absorption, @1550nm

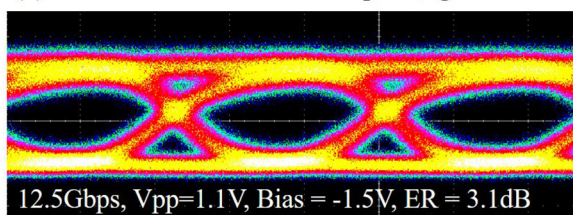


FIG. 6. Measured $2^{31}-1$ PRBS NRZ eye diagrams at 1.55 μm (a) 1.25 Gbps at forward bias 0.6 V. (b) 12.5 Gbps at reverse bias -1.5 V.

transient energy consumption for this EAM is 0.29 fJ/bit. The transient energy consumption can be further reduced by narrowing the MQW+SCH layer width, which effectively decreases the junction capacitance. The DC energy consumption per bit at 1.25 Gbps is 110 fJ/bit, which can be reduced by increasing the modulator speed. It is worthwhile noting that the rise and fall time is limited by the carrier lifetime in the MQWs for the present EAM working under a forward bias. Fig. 6(b) shows the high-speed performance for the same EAM working under a reverse bias at a data rate of 12.5 Gbps with a voltage swing of 1.1 V. One can see that the modulation bandwidth is significantly increased due to the fact that the carrier lifetime is largely reduced at a reverse bias. The speed of the EAM in this case is limited by the RC time constant.^{1,9} Using modulation-doped MQWs to move the Fermi energy level above the lowest confined state in the conduction band at zero bias, we can shift the working point to a reverse bias.^{13,16} In this way, the modulation bandwidth of the present band-filling based EAM can also be increased.

In summary, we have demonstrated an III-V-on-silicon EAM based on the band filling effect. With 100 mV bias variation, the DC extinction ratio is better than 20 dB. The exciton absorption peak shift and intensity variation are in good agreement with the simulation results. A clear open eye diagram has been obtained at 1.25 Gbps with a dynamic extinction ratio of 6.3 dB. The peak-to-peak driving voltage is only 50 mV. The speed of the present device is limited by carrier lifetime and can be further improved by using modulation-doped MQWs. The insertion loss and transient energy consumption can be further improved with optimized fabrication processes.

This work was partially supported by the National Natural Science Foundation of China (91233208 and 61377038), the National High-Tech R&D Program of China (Grant No. 2013AA014401), the Guangdong Innovative Research Team Program (201001D104799318), the China Scholarship Council (award to Qiangsheng Huang, Yingchen Wu, and Xin Fu for 1 years study abroad at Ghent University), and the European Commission through the ERC-project ULPPIC.

¹Y. Tang, J. D. Peters, and J. E. Bowers, *IEEE Photonics Technol. Lett.* **24**, 1689 (2012).

²H. Fukano, T. Yamanaka, M. Tamura, and T. Kondo, *J. Lightwave Technol.* **24**, 2219 (2006).

³R. B. Welstand, S. A. Pappert, C. K. Sun, J. T. Zhu, Y. Z. Liu, and P. K. L. Yu, *IEEE Photonics Technol. Lett.* **8**, 1540 (1996).

⁴K. Chen, Q. Huang, J. Zhang, J. Cheng, X. Fu, C. Zhang, K. Ma, Y. Shi, D. V. Thourhout, G. Roelkens *et al.*, *IEEE Photonics J.* **8**, 1 (2016).

⁵P. Zhou, S. Pan, D. Zhu, R. Guo, F. Zhang, and Y. Zhao, *IEEE Photonics Technol. Lett.* **26**, 86 (2014).

⁶D. Marpaung, C. Roeloffzen, R. Heideman, A. Leinse, S. Sales, and J. Capmany, *Laser Photonics Rev.* **7**, 506 (2013).

⁷C. Sun, M. T. Wade, Y. Lee, J. S. Orcutt, L. Alloati, M. S. Georgas, A. S. Waterman, J. M. Shainline, R. R. Avizienis, S. Lin *et al.*, *Nature* **528**, 534 (2015).

⁸G. Roelkens, A. Abassi, P. Cardile, U. Dave, A. De Groote, Y. de Koninck, S. Dhoore, X. Fu, A. Gassenq, N. Hattasan *et al.*, *Photonics* **2**, 969 (2015).

⁹X. Fu, J. Cheng, Q. Huang, Y. Hu, W. Xie, M. Tassaert, J. Verbist, K. Ma, J. Zhang, K. Chen *et al.*, *Opt. Express* **23**, 18686 (2015).

¹⁰S. Manipatruni, K. Preston, L. Chen, and M. Lipson, *Opt. Express* **18**, 18235 (2010).

- ¹¹A. Shakoob, K. Nozaki, E. Kuramochi, K. Nishiguchi, A. Shinya, and M. Notomi, *Advanced Photonics for Communications* (Optical Society of America, San Diego, California United States, 2014), p. IW3A.6.
- ¹²X. Gu, S. Shimizu, T. Shimada, A. Matsutani, and F. Koyama, *Appl. Phys. Lett.* **102**, 031118 (2013).
- ¹³G. Livescu, D. A. Miller, D. Chemla, M. Ramaswamy, T. Chang, N. Sauer, A. Gossard, and J. English, *IEEE J. Quantum Electron.* **24**, 1677 (1988).
- ¹⁴Y. Ikku, M. Yokoyama, O. Ichikawa, M. Hata, M. Takenaka, and S. Takagi, *Opt. Express* **20**, B357 (2012).
- ¹⁵T. Chang, J. Zucker, K. Jones, N. Sauer, B. Tell, M. Wegener, and D. Chemla, in Second International Conference on Indium Phosphide and Related Materials, 1990 (IEEE, 1990), pp. 447–448.
- ¹⁶V. S. Kalinovsky, T. V. Shubina, I. Yu. Shvechikov, and A. A. Toropov, *J. Phys. III France* **3**, 1021 (1993).
- ¹⁷See <http://www.epixfab.eu/> for more information about ePIXfab Multi Project Wafer run; accessed 5 January 2015 (last accessed 28 January 2016).
- ¹⁸Q. Huang, J. Cheng, L. Liu, Y. Tang, and S. He, *Appl. Opt.* **54**, 4327 (2015).
- ¹⁹P. J. Mares and S. L. Chuang, *J. Appl. Phys.* **74**, 1388 (1993).
- ²⁰E. H. Li, *Phys. E* **5**, 215 (2000).
- ²¹L. A. Coldren and S. W. Corzine, *Diode Lasers and Photonic Integrated Circuits*, 1st ed. (John Wiley & Sons, Inc., New York, 1995), Chap. 7, pp. 414–415.